Manuscript Details

Manuscript number JCSR_2017_459

Title Initial rotational stiffness of RHS joints with axial force in main member

Abstract

In the frame analysis, the local analysis model of the joint must follow the behavior of the joint. When completing the elastic global analysis, the initial rotational stiffness of the joints should be known to obtain the reliable moment distribution between the members of the frame. This paper evaluates the existing calculation approach for the initial rotational stiffness of welded rectangular hollow section T joints. Validation with the experiments shows that the current calculation approach significantly underestimates their initial rotational stiffness. Based on the existing experimental data, the paper proposes the improvement for determining the initial stiffness. The second part of the article investigates the effect of the axial force in the main member on the initial rotational stiffness of the joint. The conducted numerical study on square hollow section T joints shows that the reduction of their initial stiffness can reach 50%, when the main member experiences the normal stresses close to yielding. Using the curve fitting approach, the paper proposes and validates a corresponding chord stress function, similar to the existing ones for the moment resistance.

Submission Files Included in this PDF

File Name [File Type]

Manuscript.pdf [Manuscript File]

To view all the submission files, including those not included in the PDF, click on the manuscript title on your EVISE Homepage, then click 'Download zip file'.

Introduction

Feasibility study dealing with safety of the structure starts from the global analysis of the structure. In the frame analysis, which is conducted using beam elements, the local analysis model of the joint must follow the behavior of the joint. In this regard, the stiffness, in this case the initial rotational stiffness, becomes the important quantity of joints. It has been shown that the significant cost savings can be achieved by considering the initial rotational stiffness of semi-rigid joints, both in sway frames [1, 2] and in non-sway frames [3]. Moreover, the rotational stiffness has the significant effect on the buckling behavior of members [4–6].

The overall research on tubular joints loaded by in-plane bending moments was conducted by Wardenier [7], who proposed the design resistance equations, which are currently presented in many design standards, such as EN 1993-1-8:2005 [8] and ISO 14346:2013 [9]. After that, the extensive studies were undertaken dealing with the strength of hollow section joints. Tabuchi et al. [10] presented the experimental results for in-plane moment loaded rectangular hollow section (RHS) T joints and examined their local failures. Szlendak [11] and Packer [12] developed the design procedures for RHS connections under the moment loading. The intensive research for uniplanar and multiplanar RHS joints was conducted by Yu [13]. The deformation limit of RHS joints was investigated by Lu [14] and Zhao [15].

In the joint, normal stresses may occur at the surface of the main member, where the connected member is located. Generally, the effect of these stresses is measured using the so-called chord stress functions, which are available for the resistances of joints in many design standards [8, 9] and handbooks [16]. The design equation for the chord stress function was originally presented in [7] for the resistance of hollow section joints. Later the considerable research was conducted worldwide dealing, however, only with the resistance of joints. The results for RHS K gap joints are provided in [17] and for RHS X and T joints in [18, 19]. The most recent study are published for RHS joints in [20] and circular hollow section (CHS) joints in [21].

At the same time, considerably less research was related to the rotational stiffness of joints. Korol & Mirza [22] described several methods to determine the behavior of joints, including the post-elastic phase. Mäkeläinen et al. [23] presented the rotational stiffness of circular hollow sections (CHS) T joints, based on the semi-analytical models. The component method, which origin can be tracked back to [24], enables to calculate the stiffness of the joint, decomposing it on the basic components. The calculation methods for the rotational stiffness of RHS T joints are presented in [25] and [26]. Both based on the component method, they employ the different mechanical models and equations to determine the stiffnesses of the components. However, in contrast to the resistance, the initial stiffness design rules were validated with the very limited amount of experimental data. Moreover, none of the presented publications considers the effect of the axial forces in the main member on the stiffnesses of the joint.

The focus of this paper is on the local initial rotational stiffness of the welded RHS T joint loaded by the in-plane bending moment. The T joint is a joint where a RHS member is connected in 90 degrees to another RHS member, called the main member. The connected member can be a brace of a truss or a beam of a frame, whereas the main member usually represents a chord of a truss or a column. Figure 1a shows the RHS T joint loaded with the in-plane moment M at the connected member and with the axial force N in the main member.

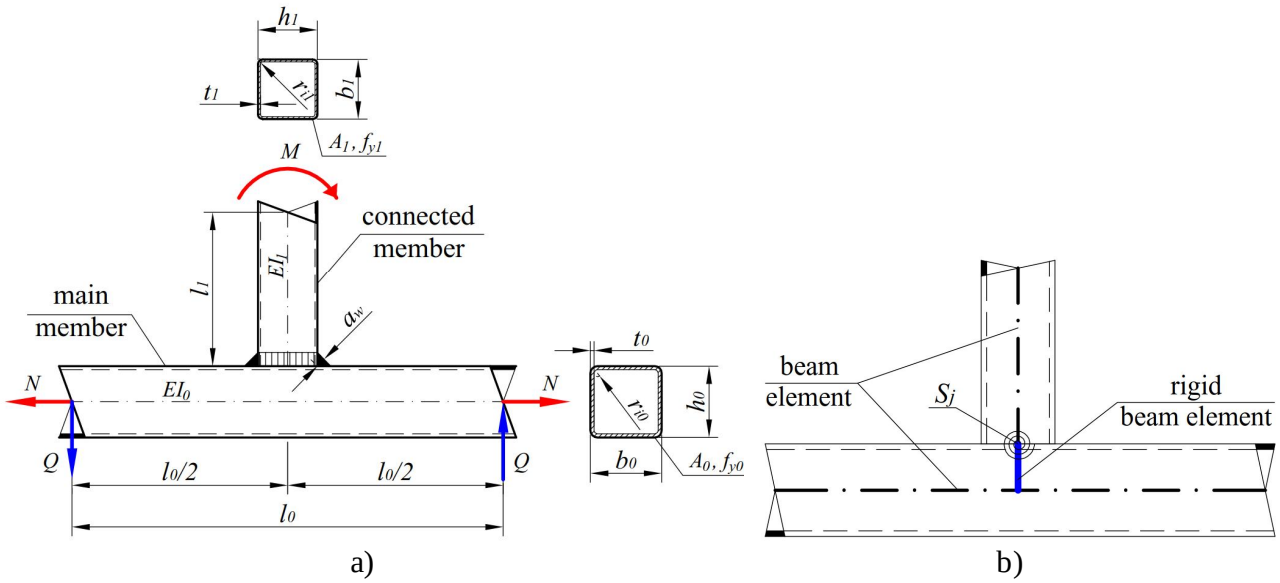

Figure 1. a) RHS T joint; b) its local design model.

As can be seen in Figure 1a, the shear forces and moments occur in the main member to compensate the moment *M*. Considering the chord stress function in the joint, it is essential to construct the test specimen and its mechanical model so that the stresses on the surface on the main member are those that they are in fact [13, 27]. On Figure 1a, the mechanical model assumes the axial stresses in the joint to be anti-symmetric with respect to the mid-line of the joint, when the axial force in the main member is zero. At the symmetric axis, the axial stresses are zero, and this is considered as the case without axial stresses in the main member.

The first section of this paper provides the theoretical background for the initial rotational stiffness of joints [25] and proposes the improved stiffness equation for one of the components. Section 2 validates the proposed improvements with the experimental data. Section 3 studies the effect of the axial force in the main member on the initial rotational stiffness and proposes the corresponding chord stress function, using the curve-fitting approach.

1. Theoretical background for the design of the initial rotational stiffness

1.1. Local analysis model

The different beam element local analysis models for welded tubular joints have been evaluated in [4] and [5]. This paper employs the best variation of [4], which is composed of the elastic and rigid beams, as presented on Figure 1b, where S_j denotes the in-plane rotational stiffness of the joint. It should be noted, that the rotation of the joint and, consequently, its rotational stiffness, are defined at the point where the member is connected to the surface of the main member, not at the intersection point of the connected and main member midlines, as is defined in [8]. The motivation for such assumption is provided in [28, 29]. This assumption is also used in [26], where it is shown that the local analysis model is situated at the surface of the main member. The properties of the beam elements should follow those they represent, i.e., the connected and main members.

1.2. Moment resistance

Generally, the initial rotational stiffness of the joint is considered as a function of the joint geometry and the elastic properties of steel. However, the authors provide also the theoretical background for the

moment resistance, to verify that the same length of the yield mechanism is used also for the initial stiffness.

Consider the moment loaded T joint with $\beta = b_1/b_0 \leq 0.85$ (Figure 2a). According to Table 7.14 of [8], the face failure is the critical failure mode for such joint, the failure mechanism of which is presented in Figure 2b.

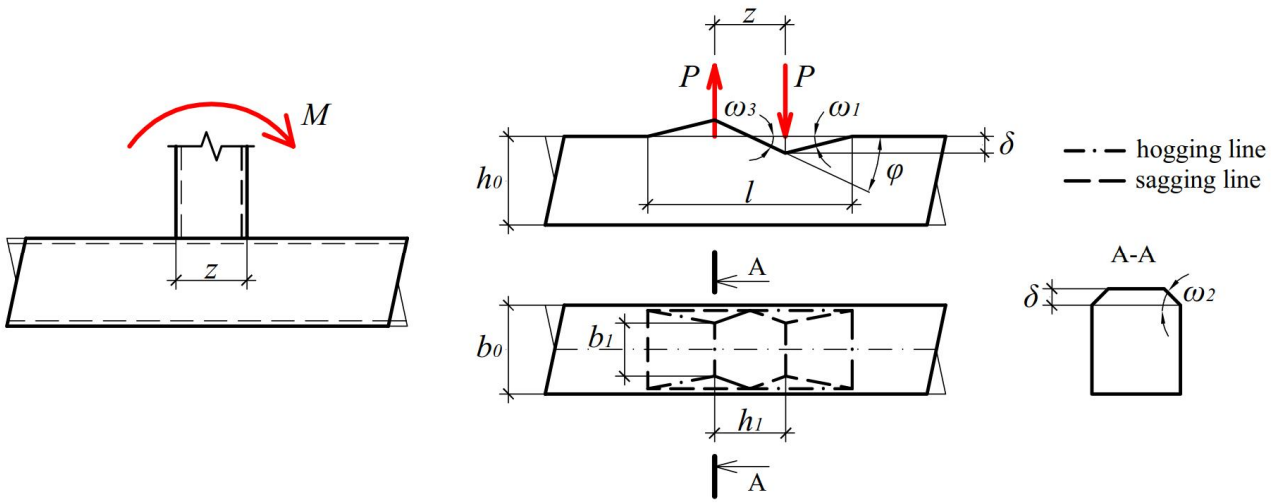

a) b)

Figure 2. a) In-plane moment loaded T joint; b) its yield mechanism.

The resistance of the in-plane moment loaded T joint can be calculated based on the classical yield line theory of Johansen [30], which is also employed in [7]. Following it, the virtual work equation of the yield mechanism can be presented as

$$M \times \varphi = \sum_{i=1}^{n} m_{pl,i} \times l_i \times \omega_i \tag{1}$$

where M is the moment load of the joint; φ is the rotation of the joint; $m_{pl,i}$ is the yield moment intensity at the yield line i; l_i is the length of the yield line i; ω_i is the rotation at the yield line i.

Consider next only a half of the mechanism shown on Figure 2b, denoting $P = M/z$, where z is the lever arm. Using the projection rule of the yield line theory, the virtual work equation of the yield mechanism can be presented as (note that no plastic work occurs at the midline of the joint)

$$P \times \delta = m_{pl} \times (2b_0\omega_1 + 4 \times (l/2) \times \omega_2 + b_0\omega_3) \tag{2}$$

where

δ is the maximum displacement at the joint;

m_{pl} is the plastic moment intensity at the yield line: $m_{pl} = 0.25 f_{y0} t_0^2$

ω_1, ω_2, ω_3 are the rotations at the yield lines;

l is the total length of the yield mechanism.

According to the geometry of the joint:

$$\omega_1 = \frac{\delta}{(l - h_1)/2}; \omega_2 = \frac{\delta}{(b_0 - b_1)/2}; \omega_3 = \frac{\delta}{h_1/2} \tag{3}$$

Following (3), Eq. (2) can be written as

$$P = 2m_{pl} \times \left[\frac{2b_0}{l - h_1} + \frac{2l}{b_0 - b_1} + \frac{b_0}{h_1} \right] = \frac{4m_{pl}}{b_0 - b_1} \times \left[\frac{b_0(b_0 - b_1)}{l - h_1} + l + \frac{b_0(b_0 - b_1)}{2h_1} \right] \quad (4)$$

The minimum load P corresponds to the critical yield load, giving the total length l of the mechanism:

$$\frac{dP}{dl} = 0 \Rightarrow -\frac{b_0(b_0 - b_1)}{(l - h_1)^2} + 1 = 0 \Rightarrow l = h_1 + \sqrt{b_0(b_0 - b_1)} \quad (5)$$

It can be seen, that this length is equal to the length of the mechanism for the axial load of the joint [7]. Implementing l to Eq. (4) and using the notation $M = Pz$, the yield moment of the joint can be obtained:

$$M = \frac{4m_{pl}z}{b_0 - b_1} \times \left[h_1 + 2\sqrt{b_0(b_0 - b_1)} + \frac{b_0(b_0 - b_1)}{2h_1} \right] = 4m_{pl}z \times \left[\frac{1}{2h} + \frac{2}{\sqrt{1 - b}} + \frac{h}{1 - b} \right] \quad (6)$$

Implementing $m_{pl} = 0.25 f_{y0} \times t_0^2$ and assuming $z = h_1$ leads to the final equation of the moment resistance, which is presented in [8] and [9] for $\beta \leq 0.85$:

$$M = f_{yo} t_0^2 h_1 \times \left[\frac{1}{2\eta} + \frac{2}{\sqrt{1 - \beta}} + \frac{\eta}{1 - \beta} \right] \quad (7)$$

For the range $0.85 \leq \beta \leq 1.0$, [8] provides the equations to check chord side wall crushing and brace failure. The effects of strain hardening and membrane action are neglected in Eq. (7), as well as the effect of the axial stresses in the chord. The verification and validation of Eq. (7) was conducted with the tests and finite element analyses in many references [7, 25, 31].

1.3. Initial rotational stiffness

The initial rotational stiffness is determined using the component method, which is currently employed by [8] for the joints connecting H and I sections. It was also applied for RHS joints in [25]. According to [8], the initial rotational stiffness of the joint, $S_{j,ini}$, is calculated as

$$S_{j,ini} = \frac{Ez^2}{\sum_i \frac{1}{k_i}}, \quad (8)$$

where E is the Young's modulus; $z = h_1$ is the lever arm; k_i is the stiffness coefficient for basic joint component i. Based on [25], the following stiffness coefficients k_i should be considered when calculating the initial stiffness of the welded RHS T joint:

- k_{cf} is the coefficient for the deformation of the main member surface, where the connected member is welded;
- k_{cw} is the coefficient for compression and tension deformation of the main member webs;
- k_{sh} is the coefficient for the shear deformation of the main member webs, denoted as k_i in [25].

Other coefficients, which relate to the weld deformations and the axial deformations of the brace, are not considered for RHS joints. Normally, the coefficient k_{cf} is the smallest, which means that the deformation of the main member face is the most essential when defining the rotational stiffness of the joint, particularly for the joints with small β.

1.3.1. Coefficient k_{cf}

Following Eq. (2.5.19) in [25], the coefficient k_{cf} is calculated as

$$k_{cf} = \frac{8t_0^3 l_{eff,cf}}{(1-\beta)^3 b_0^3} \times \frac{1}{2+\frac{6\beta}{1-\beta}} \tag{9}$$

This equation has been derived using the Euler-Bernoulli beam theory, considering the one-span simply supported beam with the length b_0 and loaded by two point forces $P/2$ with the distance b_1 (Figure 3). The width and the thickness of the beam are $l_{eff,cf}$ and t_0 correspondingly.

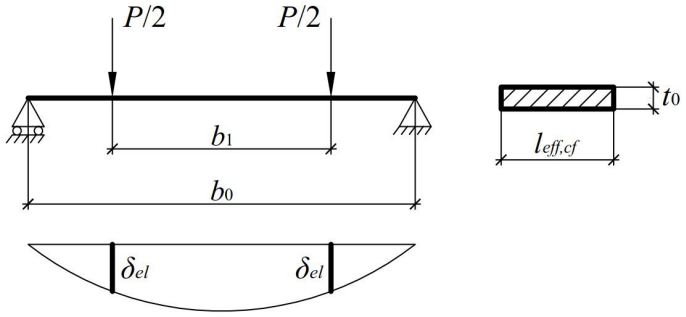

Figure 3. Beam model for the coefficient k_{cf}.

The deflection δ_{el} of the beam at the point load is

$$\delta_{el} = \frac{P}{48EI} \times (b_0 - b_1)^2 \times (b_0 + 2b_1) \tag{10}$$

Assuming $I = \frac{t_0^3 \times l_{eff,cf}}{12}$, δ_{el} can be presented as

$$\delta_{el} = \frac{P}{4Et_0^3 l_{eff,cf}} \times (b_0 - b_1)^2 \times (b_0 + 2b_1) \tag{11}$$

The coefficient k_{cf}:

$$k_{cf} = \frac{P}{E\delta_{el}} = \frac{4t_0^3 l_{eff,cf}}{(b_0 - b_1)^2 \times (b_0 + 2b_1)} = \frac{8t_0^3 l_{eff,cf}}{(b_0 - b_1)^3 \times \left(2 + 6\frac{b_1}{b_0 - b_1}\right)} = \frac{8t_0^3 l_{eff,cf}}{(1-\beta)^3 b_0^3} \times \frac{1}{2+\frac{6\beta}{1-\beta}} \tag{12}$$

Table 2.5.1 in [25] presents two options for calculating the effective width $l_{eff,cf}$:

$$l_{eff,cf} = t_1 + 2 \times b_0 \sqrt{1-\beta} \tag{13}$$

$$l_{eff,cf} = \frac{h_1}{2} + b_0 \times \sqrt{1-\beta} \tag{14}$$

Based on the classical yield line theory, it can be seen that Eq. (13) represents the length of the total yield line pattern for the perpendicular line load at the surface of the chord. However, Eq. (14) is not the half of the length of the total yield pattern, compare to Eq. (5). In this paper, Eq. (13) is used to determine the effective width.

The local design model of the joint consists of the compressive and tensile parts (Figure 2), which are assumed to behave similarly [25]. Therefore, the coefficient k_{cf} can be used also for the tensile part of the model and thus is counted twice in Eq. (8).

After the validation with the experimental data, it was found that Eq. (9) significantly underestimates the stiffness of the component, leading thus to very conservative results of the overall initial rotational

stiffness. To avoid this, a more accurate solution was proposed in Eq. (15). The justification for that is presented in Section 2.

$$k_{cf} = \frac{20 t_0^3 l_{eff,cf}}{(1-\beta)^3 b_0^3} \times \frac{1}{2 + \frac{6\beta}{1-\beta}} \tag{15}$$

1.3.2. Coefficient k_{cw}

Following clause 2.6.2 of [25], the coefficient k_{cw} is defined as

$$k_{cw} = \frac{2 \times t_0 \times b_{eff,cw,el}}{h_0 - 3t_0} \tag{16}$$

where

$$b_{eff,cw,el} = 2 \times 0.7 \times l_{eff,cw} + t_1 \tag{17}$$

$$l_{eff,cw} = \max \begin{cases} t_0 \times \sqrt{\frac{b_0}{2 \times t_0}} \le 2.5 \times t_0 \\ \frac{b_0}{2} \times \sqrt{1-\beta} \le \frac{h_0}{2} \end{cases} \tag{18}$$

The first part of Eq. (18) limits the spread of the yield to $2.5t_0$ at both sides of the flange of the brace, while the origin of the second part comes from the yield condition. Similarly to k_{cf}, the coefficient k_{cw} is the same in tension and compression and is taken into account twice in Eq. (8).

1.3.3. Coefficient k_{sh}

According to clause 6.11 of [8], the shear coefficient k_{sh} is determined as

$$k_{sh} = 0.38 \times \frac{A_{VC}}{r z} \tag{19}$$

where $r \approx 1$ is the transformation parameter (Table 5.4, [8]), z is the lever arm and, following Eq. (2.7.8) in [25], the shear area is:

$$A_{VC} = 2 t_0 (h_0 - t_0) \tag{20}$$

The coefficient k_{sh} is taken into account only once in Eq. (8).

1.3.4. Initial rotational stiffness

Taking into account all the above, the initial rotational stiffness is calculated as

$$S_{j,ini} = \frac{E z^2}{\frac{2}{k_{cf}} + \frac{2}{k_{cw}} + \frac{1}{k_{sh}}} \tag{21}$$

2. Validation of the initial rotational stiffness for RHS T joints

This section validates the calculation approach for the initial rotational stiffness with the experimental tests available in the literature. The theoretical initial rotational stiffness $S_{j,ini}$ is compared to the experimental value $S_{j,ini,exp}$. For the theoretical values, the coefficient k_{cf} is calculated using both Eq. (9), presented in [25], and the proposed Eq. (15).

2.1. HAMK tests

Consider first the tests of [32], which represent twenty experiments of HSS square hollow section T joints with varying section dimensions, steel grades, weld sizes and welding types (Table 1). It can be seen that the original approach, Eq. (9), considerably underestimates the initial rotational stiffness of the joints. Oppositely, Eq. (15) provides more accurate prediction, particularly for the butt-welded joints. However, for the joints with fillet welds, the results are still underestimated.

Table 1. HAMK tests. For $S_{j,ini}/S_{j,ini,exp}$: absolute values, average value and (standard deviation).

Case	Main member	Connected member	a_w [mm]	β	$S_{j,ini}$ [kNm/rad]		$S_{j,ini,exp}$ [kNm/rad]	$S_{j,ini}$ / $S_{j,ini,exp}$			
					Eq. (9)	Eq. (15)		Eq. (9)		Eq. (15)	
1111	150x150x8	100x100x8	6	0.66	401	913	1115	0.36		0.82	
2111	150x150x8	100x100x8	6	0.67	422	956	1083	0.39		0.88	
2211	150x150x8	100x100x8	6	0.67	421	954	995	0.42	0.39	0.96	0.87
3111	150x150x8	100x100x8	6	0.67	405	919	1082	0.37	(0.06)	0.85	(0.10)
3211	150x150x8	100x100x8	6	0.67	403	916	1108	0.36		0.83	
3214	150x150x8	100x100x8	6	0.67	403	916	1282	0.31		0.71	
3311	150x150x8	120x120x8	6	0.80	1030	2113	1990	0.52		1.06	
1121	150x150x8	100x100x8	10	0.67	407	924	1692	0.24		0.55	
2121	150x150x8	100x100x8	10	0.67	423	958	1701	0.25		0.56	
2221	150x150x8	100x100x8	10	0.67	424	959	1452	0.29		0.66	
3121	150x150x8	100x100x8	10	0.67	397	903	1521	0.26	0.29	0.59	0.64
3221	150x150x8	100x100x8	10	0.67	401	913	1705	0.24	(0.07)	0.54	(0.13)
3224	150x150x8	100x100x8	10	0.67	399	908	1455	0.27		0.62	
3321	150x150x8	120x120x8	10	0.80	1048	2141	2268	0.46		0.94	
1131	150x150x8	100x100x8	butt	0.67	414	940	893	0.46		1.05	
2131	150x150x8	100x100x8	butt	0.67	424	960	977	0.43		0.98	
2231	150x150x8	100x100x8	butt	0.67	425	961	1003	0.42	0.45	0.96	1.00
3131	150x150x8	100x100x8	butt	0.67	401	911	971	0.41	(0.05)	0.94	(0.06)
3231	150x150x8	100x100x8	butt	0.67	409	930	961	0.43		0.97	
3331	150x150x8	120x120x8	butt	0.81	1100	2222	1990	0.55		1.12	

2.2. Tests of TH Karlsruhe and Kobe University

The next validation (Table 2) is conducted using the results of the TH Karlsruhe [33] and the Kobe University [34]. The initial rotational stiffnesses are extracted from the moment-rotation curves (Figures 4 and 5), provided in [25]. As in the case with HAMK tests, the calculation is much more accurate, if Eq. (15) is used instead of Eq. (9).

Table 2. Tests of the TH Karlsruhe and the Kobe University. For $S_{j,ini}/S_{j,ini,exp}$: absolute values, average value and (standard deviation).

Case	Main member	Connected member	a_w [mm]	β	$S_{j,ini}$ [kNm/rad]		$S_{j,ini,exp}$ [kNm/rad]	$S_{j,ini}$ / $S_{j,ini,exp}$			
					Eq. (9)	Eq. (15)		Eq. (9)		Eq. (15)	
M44	160x160x4	100x100x3	3	0.63	41	100	130	0.31		0.77	
M45	160x160x5	100x100x3	3	0.63	79	191	260	0.30	0.35	0.73	0.82
S12	200x200x9	150x150x6	6	0.75	1043	2325	2000	0.52	(0.10)	1.16	(0.20)
S23	250x250x6	175x175x6	6	0.70	226	550	875	0.26		0.63	

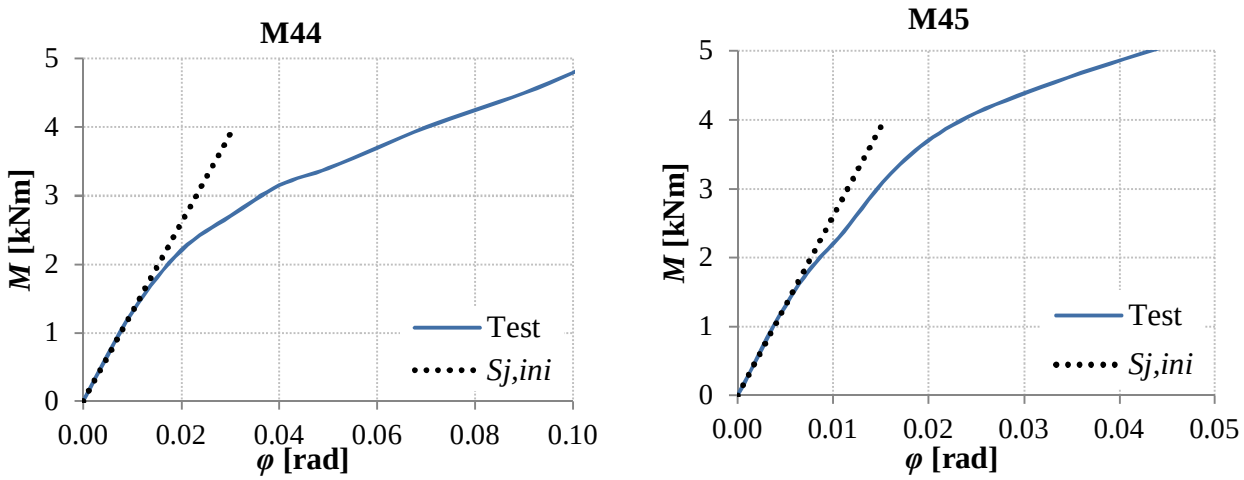

Figure 4. Initial rotational stiffness extracted from the tests of the TH Karlsruhe, [25], Annex B.3.

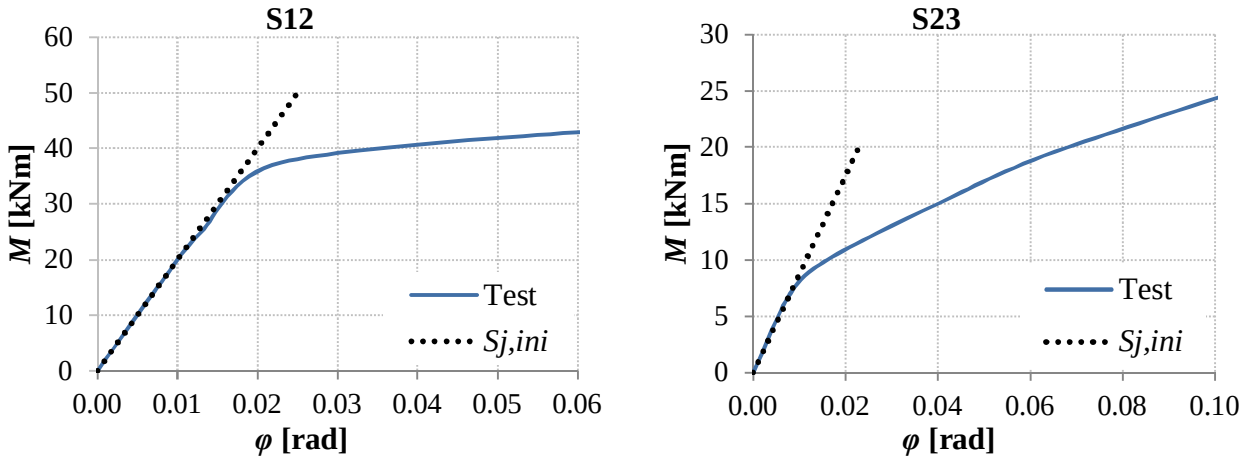

Figure 5. Initial rotational stiffness extracted from the tests of the Kobe University, [25], *Annex B.4.*

2.3. Tests of Christitsas et al.

This validation is conducted using the tests of [31], which present the experimental stiffness of the square hollow section X joints subject to in-plane bending moment (Table 3). The results are in line with the previous observations: Eq. (15) yields more accurate prediction of the initial rotational stiffness.

Table 3. Tests of Christitsas et al. For $S_{j,ini}/S_{j,ini,exp}$: absolute values, average value and (standard deviation).

Case	Main member	Connected member	a_w [mm]	β	$S_{j,ini}$ [kNm/rad]		$S_{j,ini,exp}$ [kNm/rad]	$S_{j,ini}$ / $S_{j,ini,exp}$			
					Eq. (9)	Eq. (15)		Eq. (9)		Eq. (15)	
80c150t5	150x150x5	80x80x5	6	0.53	46	111	135	0.34		0.82	
80c150t6	150x150x6	80x80x5	6	0.53	78	189	208	0.38		0.91	
80c150t8	150x150x8	80x80x5	6	0.53	183	430	407	0.45		1.06	
100c150t5	150x150x5	100x100x5	6	0.67	104	249	301	0.34		0.83	
100c150t6	150x150x6	100x100x5	6	0.67	177	417	494	0.36	0.41 (0.08)	0.84	0.94 (0.17)
100c150t8	150x150x8	100x100x5	6	0.67	408	924	712	0.57		1.30	
120c150t5	150x150x5	120x120x5	6	0.80	279	634	741	0.38		0.86	
120c150t6	150x150x6	120x120x5	6	0.80	469	1028	1366	0.34		0.75	
120c150t8	150x150x8	120x120x5	6	0.80	1041	2119	1927	0.54		1.10	

2.4. Discussion concerning initial stiffness

As can be seen from the validation results, Eq. (9), originally proposed in [25], provides very conservative results: the $S_{j,ini} / S_{j,ini,exp}$ ratio is 0.29…0.45 for HAMK tests, 0.35 for the TH Karlsruhe and the Kobe University and 0.41 for the tests of Christitsas et al. Oppositely, Eq. (15) provides considerably more accurate values, with the $S_{j,ini} / S_{j,ini,exp}$ ratio close to one.

Comparing the results of HAMK tests, it can be noted that the joints with fillet welds have significantly higher initial stiffness than those with butt welds, in average 13% higher for the 6 mm weld joints and 36% higher for the 10 mm weld joints. This allows making a conclusion that fillet welds significantly affect the initial rotational stiffness of joints. This corresponds well with the results of [35], who proposed a simple rule to calculate the initial rotational stiffness of Y joints using the equivalent brace width:

$$b_{1,eq} = b_1 + 2\sqrt{2}a_w k_{fw} \tag{22}$$

where a_w is the fillet weld size, k_{fw} is a correlation coefficient, determined as 0.6 for S355 and 0.7 for S700. Overall, Eq. (22) leads to the additional width of $(0.6...0.7)\times\sqrt{2}a_w$ at both sides of the connected member, which is very close to the proposal $0.8\times\sqrt{2}a_w$ for open cross-sections in Figure 6.8 of [8].

3. Chord stress function for initial rotational stiffness

The axial forces acting in the main member are known to reduce the resistance of the joint [7]. This reduction is defined by the chord stress functions, the simplest of which, Eq. (23), is presented in [8]. The extensive research on the chord stress functions for RHS joints is also provided in [18, 19].

$$k_n = \begin{cases} 1.3 - \dfrac{0.4|n|}{b} \le 1.0, & n > 0 \\ 1.0, & n < 0 \end{cases} \tag{23}$$

where n is the ratio of the normal stress in the main member to its yield strength:

$$n = \frac{\sigma_0}{f_{y0}} = \frac{N_0}{A_0 f_{y0}} + \frac{M_0}{W_{el0} f_{y0}} = \frac{N_0}{A_0 f_{y0}} \tag{24}$$

where A_0 is the cross-sectional area of the main member and N_0 is the axial load in the main member. In [8], negative n means tension in the main member, while the positive one indicates compression. However, many publications [18, 19, 21] employ for n the inverse order, which is also used in this paper.

As has been proposed in [36], the similar phenomenon can be also observed for the initial stiffness of joints. Although in predominantly statically loaded trusses there is no need to take into account joint stiffnesses for the load distribution if the critical parts have sufficient rotation capacity, in frame structures stiffnesses of joints have to be considered in the global analysis. From that point of view, such an effect can lead to the noticeable redistribution of forces in the members of frames, making the results of the analysis unreliable. This fact justifies the necessity to develop the chord stress function for the initial stiffness of joints. For that reason, Eq. (8) should be presented in the following way:

$$S_{j,ini} = \frac{k_{sn,ip} E z^2}{\sum_i \dfrac{1}{k_i}}, \tag{25}$$

where $k_{sn,ip}$ is the chord stress function for the initial rotational stiffness.

This section evaluates the effect of the axial force in the main member on the initial in-plane rotational stiffness of hollow section T joints. On the first step, the FEM analysis is conducted to investigate the

effect of the chord stress on the initial stiffness. The obtained results are then approximated using the linear and polynomial regressions, proposing the final chord stress function.

3.1. FEM

The numerical analyses were performed with the FE package ABAQUS/Standard [37]. The scope of the study was restricted to square hollow sections, since RHS joints would have required considering the extra variable b_0/h_0, thus leading to the significant increase of the sample points. The FEM analyses were conducted for a single main member size 300x300. Following the requirements of the [8], the main member wall thickness t_0 varied from 8.5 mm (2γ = 35) to 30 mm (2γ = 10), whereas the connected member width changed from 75 mm (β = 0.25) to 300 mm (β = 1.00), see Table 4. The wall thickness t_1 of the connected member was chosen so that it did not exceed the thickness of the main member t_0. All the sections were modeled with round corners, according to [38], meaning cold-formed sections. To exclude the possible effects of the main member end conditions, its length was selected as $10b_0$, as recommended in [39], while the connected member length was chosen as $4b_1$, following [13]. The relative stress in the main member, n, was determined using Eq. (24).

Table 4. FEM parameters.

Main member	$300 \times 300 \times t_0$						
	t_0 [mm]	8.5	10	12	15	20	30
	2γ	35	30	25	20	15	10
Connected member	$b_1 \times b_1 \times t_1$						
	b_1 [mm]	75	150	225	255	300	
	β	0.25	0.50	0.75	0.85	1.00	
n	-0.99, -0.98, -0.95, -0.80, -0.60, -0.4, -0.2, 0, 0.2, 0.4, 0.6, 0.8, 0.95, 0.99						

The sections were modelled using 20-noded solid quadratic finite elements with reduced integration (C3D20R in Abaqus), with two elements in thickness direction (Figure 6a). Since the deformation of the main member top face represents the dominating failure mode, its mesh was refined closer to the connected face (Figure 6a). Figure 6b illustrates the boundary conditions of the FE model. The T joints were modelled with butt welds, meaning no welds, using the tie constraint of Abaqus (Figure 7a), which ties two separate surfaces together so that there is no relative motion between [37]. This approach allows using individual meshes for the main and connected members without matching their nodes (Figure 7b) and is employed by many researchers [40, 41]. The joints with β = 1.0 were modelled with the end preparations of the connected member (Figure 7c).

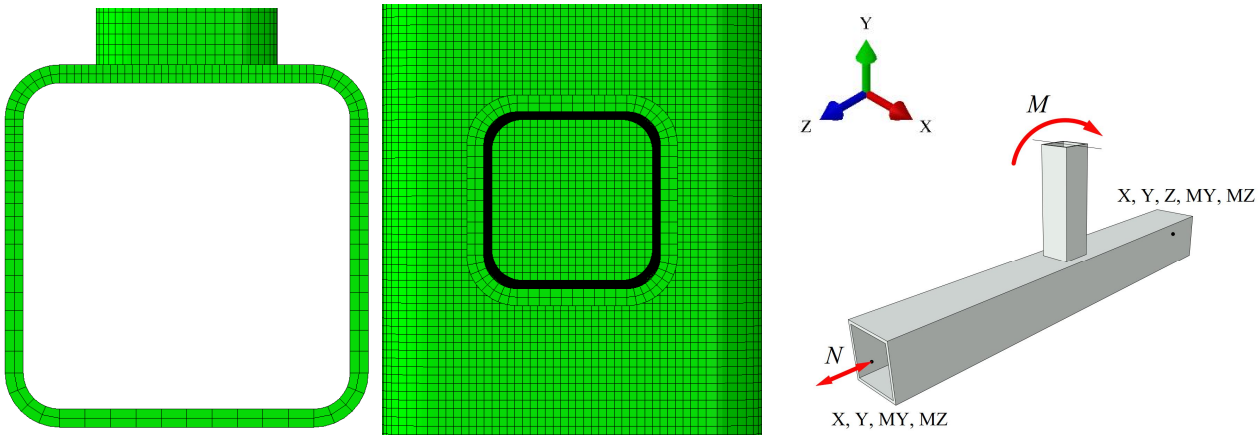

a) *b)*

Figure 6. a) meshing; b) boundary conditions.

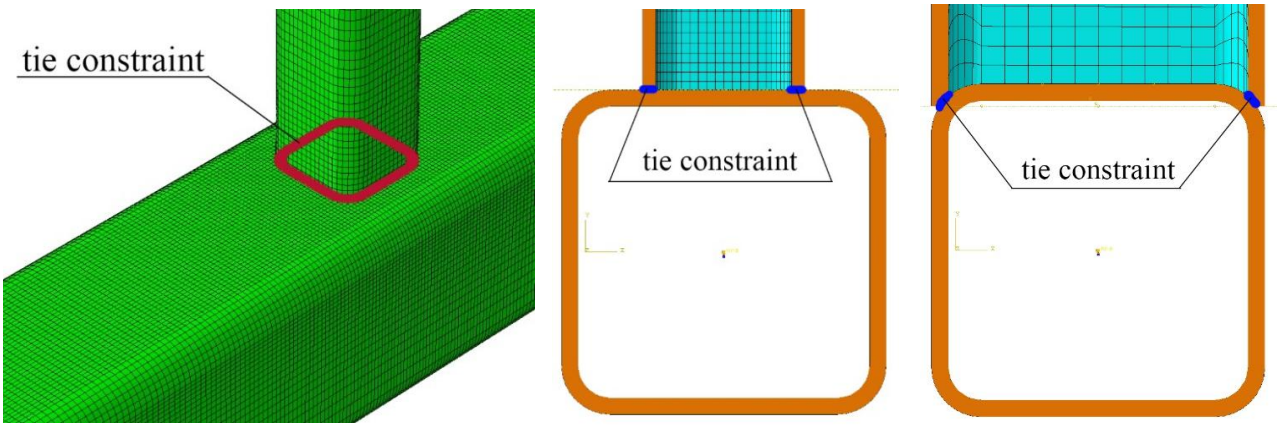

a) b) c)

Figure 7. a) Tie constraint; b) FE model for β = 0.50; c) FE model for β = 1.0.

The analyses were conducted in two steps: after the axial load was applied to the main member on the first step, the end of the connected member was loaded with the concentrated in-plane moment M_{ip} using only one increment, corresponding approximately to 0.1 rad and meaning no yielding at the joint area. All calculations employed the same ideal plastic material model for S500 steel, with E = 210 GPa and ν = 0.3. The outcome of the FEM was the overall rotation in the end of the connected member φ_{FEM}. To obtain the rotation φ_j corresponding to the in-plane rotational stiffness $S_{j,ini}$, φ_{FEM} was reduced by the rotation of the brace φ_{br} and the rotation of the chord φ_{ch}:

$$j_j = j_{FEM} - j_{br} - j_{ch} \tag{26}$$

The rotation of the brace is

$$j_{br} = \frac{M_{ip} l_1}{E I_{1,ip}} \tag{27}$$

where l_1 and $I_{1,ip}$ are the length and the in-plane moment of inertia of the brace, respectively.

The rotation of the chord is

$$j_{ch} = \frac{M_{ip} l_0}{12 E I_{0,ip}} \tag{28}$$

where l_0 and $I_{0,ip}$ are the length and the in-plane moment of inertia of the chord, respectively.

Finally, the initial rotational stiffness can be presented as

$$S_{j,ini} = \frac{M_{ip}}{j_j} \tag{29}$$

The observed influence of the axial force in the main member on the initial rotational stiffness was found to have the similar pattern as in the case with the moment resistance, as depicted in Figures 8 and 9. According to the graphs, the reduction of the stiffness can be extremely high, more than 50% for the joints with small β and large γ. Similarly, for the same joints, the increase of the initial stiffness can reach 30%. For $-0.8 \le n \le 0.8$, the response is generally linear, being nonlinear when $0.8 < |n| \le 0.99$. In addition, the effect was observed to weaken with the increase of β and the decrease of γ. For the joints with β = 1.0, the dependence on γ is negligibly little.

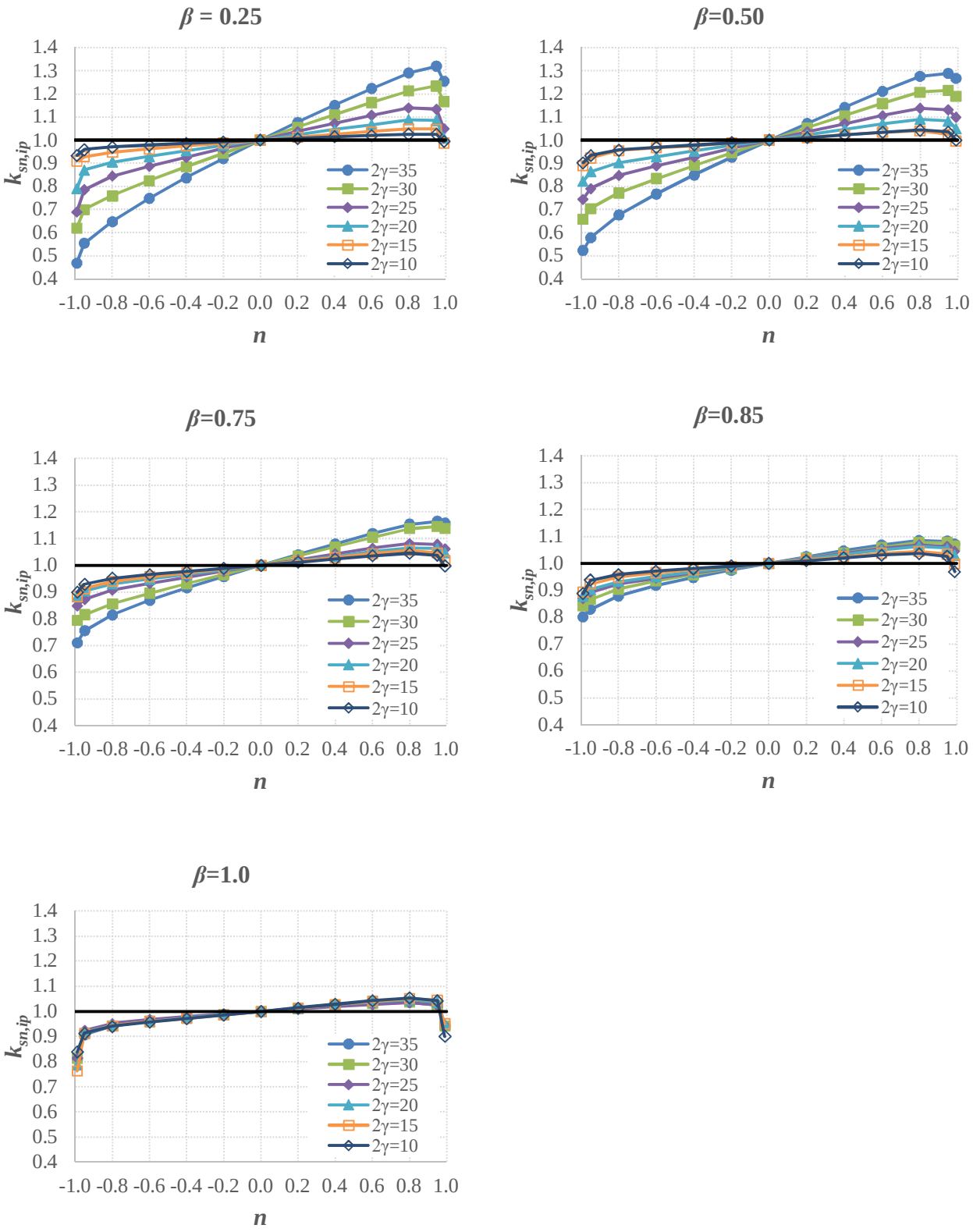

Figure 8. Chord stress function depending on γ. The function weakens with the decrease of γ. For β=1.0, the difference is negligibly little.

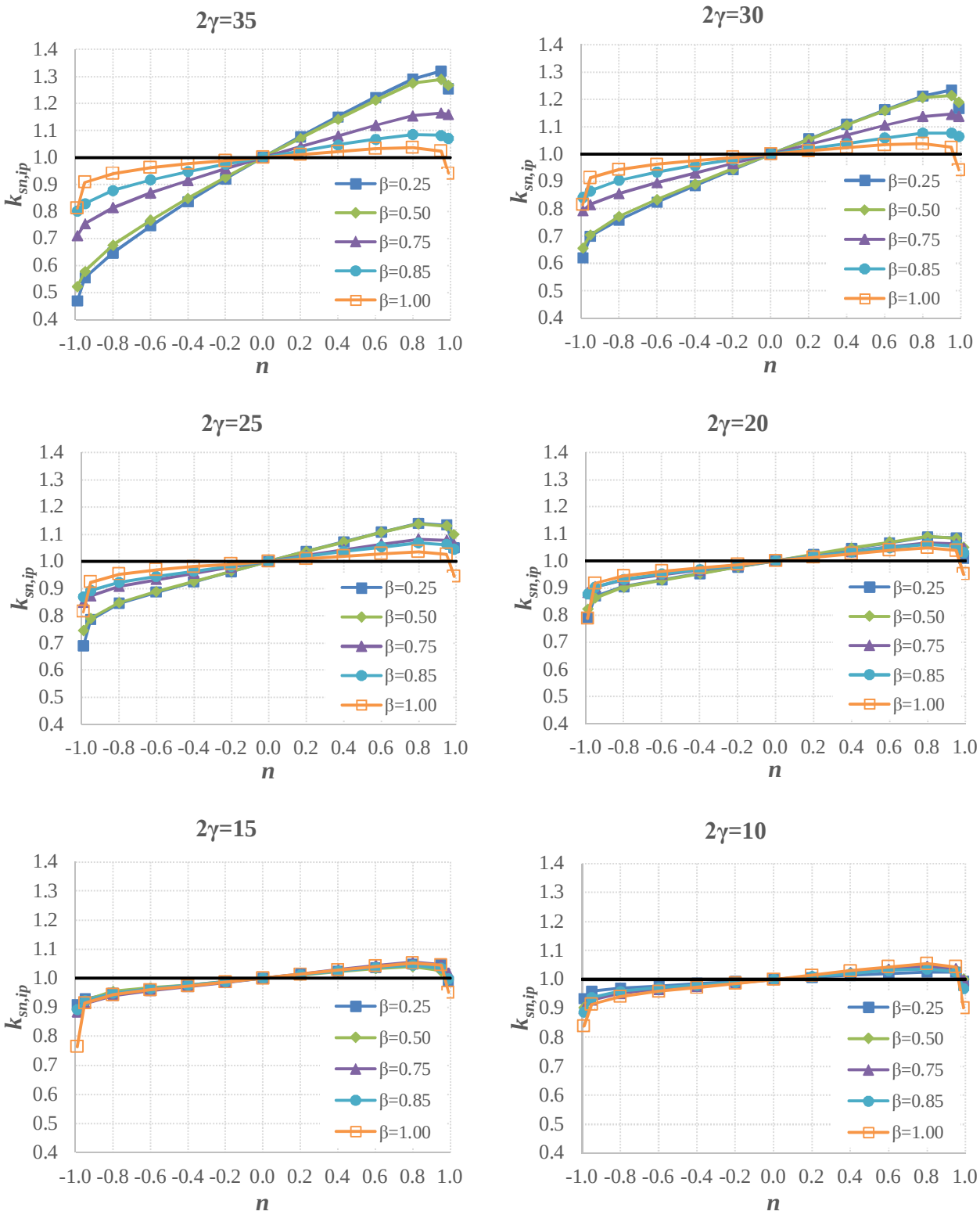

Figure 9. Chord stress function depending on β. The function weakens with the increase of β. For small γ (2γ=15 and 2γ=10), the difference is negligibly little.

3.2. Chord stress function for initial rotational stiffness

To take into account the effect of the axial stresses in the main member on the initial rotational stiffness of the joint, the corresponding chord stress function was developed using the obtained numerical results. Following the above observations, the function was found dependent on three variables: β, γ and n. To compare the values of the proposed function with the FEM results, the coefficient of determination R^2, the average percent error Δ_{av} and the maximum percent error Δ_{max} were selected as the assessment criteria. On the first step, the existing chord stress functions for the moment resistance were tested for applicability to the case of the initial stiffness.

3.2.1. Existing chord stress functions for moment resistance

As a starting point for the approximation, the current chord stress function in [8] was selected, Eq. (23) (Case 1). Since it does not consider the increase of the stiffness for $n > 0$, it was found to provide very inaccurate results (Table 5). Case 2, the development of Case 1 extended also for positive n, did not bring reasonable results. The similar performance was obtained for the chord stress functions proposed in [19], Cases 3 and 4, and [18], Cases 5 and 6. None of these functions considers the increase of stiffness for $n > 0$, and thus cannot be extended for the initial stiffness.

Table 5. Approximation based on the existing chord stress functions for the moment resistance.

Case	Equation	A	B	C	R^2	Δ_{av} [%]	Δ_{max} [%]
1	$k_{sn,ip} = \begin{cases} 1.3 - \dfrac{0.4\lvert n\rvert}{b} \le 1.0, & n < 0 \\ 1.0, & n > 0 \end{cases}$	-	-	-	0.34	12.7	160.5
2	$k_{sn,ip} = 1 + A\dfrac{n}{b+B}, -0.99 \le n \le 0.99$	0.419	0.917	-	0.63	10	37.1
3	$k_{sn,ip} = \begin{cases} (1 - \lvert n\rvert)^{0.6 - 0.5b}, & n < 0 \\ (1 - \lvert n\rvert)^{0.1}, & n > 0 \end{cases}$	-	-	-	0.32	20.9	88.0
4	$k_{sn,ip} = (1+n)^{A+Bb}$	-0.148	0.031	-	0.25	13.6	93.2
5	$k_{sn,ip} = (1 - n^2)^{0.8 - 0.8b + 0.01g}$	-	-	-	0.04	26.0	96.0
6	$k_{sn,ip} = (1 - n^2)^{A+Bb+Cg}$	0.018	-0.035	0.004	0.05	7.8	55.7

3.2.2. Proposed chord stress function

This section develops a chord stress function for the initial stiffness, using the stated above assessment criteria. Following the numerical observations, the approximation was assumed consisting of a linear and two nonlinear parts (Figure 10), with the following corresponding equations:

$$k_{sn,ip} = \begin{cases} 1 + A \times f(b) \times n \times g^B - C_1 \times (\lvert n\rvert - 0.8)^2, & -0.99 \le n < -0.8 \\ 1 + A \times f(b) \times n \times g^B, & -0.8 \le n \le -0.8 \\ 1 + A \times f(b) \times n \times g^B - C_2 \times (n - 0.8)^2, & 0.8 < n \le 0.99 \end{cases} \quad (30)$$

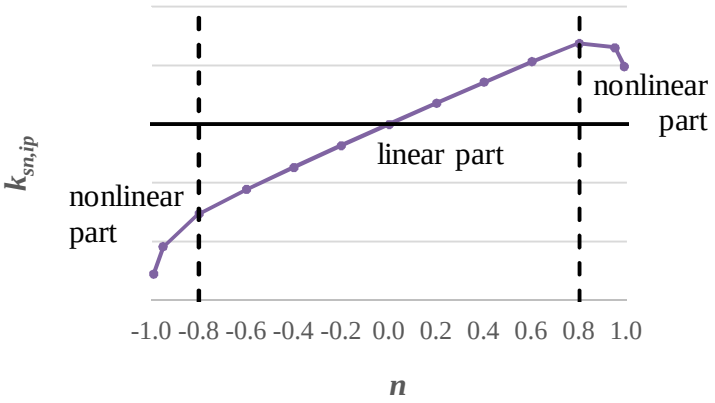

Figure 10. Approximation model for the chord stress function.

Analyzing the FEM results, $B = 2$ in Eq. (30) was found to provide the most accurate approximation for $0.25 \le \beta \le 0.85$; whereas for the joints with $\beta = 1.0$, the function was observed not to depend on γ. From that point of view, the curve fitting was conducted separately for the joints with $0.25 \le \beta \le 0.85$ and $\beta = 1.0$, proposing the linear interpolation for $0.85 < \beta < 1.0$. Eq. (31) presents the final chord stress function with the following parameters: $R^2 = 0.95$, $\Delta_{av} = 1.8\%$, $\Delta_{max} = 9.3\%$.

For $0.25 \le \beta \le 0.85$:

$$k_{sn,ip} = \begin{cases} 1 + 0.001 \times (1 + 1.7\beta - 2.6\beta^2) \times n \times \gamma^2 - 2.7 \times (|n| - 0.8)^2, & -0.99 \le n < -0.8 \\ 1 + 0.001 \times (1 + 1.7\beta - 2.6\beta^2) \times n \times \gamma^2, & -0.8 < n < 0.8 \\ 1 + 0.001 \times (1 + 1.7\beta - 2.6\beta^2) \times n \times \gamma^2 - 3.1 \times (n - 0.8)^2, & 0.8 < n \le 0.99 \end{cases}$$

For $0.85 < \beta < 1.0$: (31)

$k_{sn,ip}$ is the linear interpolation between $\beta = 0.85$ and $\beta = 1.0$

For $\beta = 1.0$:

$$k_{sn,ip} = \begin{cases} 1 + 0.06 \times n - 3.5 \times (|n| - 0.8)^2, & -0.99 \le n < -0.8 \\ 1 + 0.06 \times n, & -0.8 < n < 0.8 \\ 1 + 0.06 \times n - 2.8 \times (n - 0.8)^2, & 0.8 < n \le 0.99 \end{cases}$$

3.3. Validation of the proposed chord stress function

The validation of the final chord stress function was conducted with the new FE results and using the same FE model. To prove that the proposed function is scalable in the main member width, two chord sizes were considered, 100x100 and 200x200, with $2\gamma = 12.5$ and $2\gamma = 25$ (Table 6). Validation was performed for two brace widths ($\beta = 0.40$ and $\beta = 0.90$) and two steel grades (S355 and S700).

The validation results are presented in Table 7 for one case and graphically in Figure 11 for all cases. As was expected, when the joints are not loaded by the axial load in the main member ($n = 0$), their initial rotational stiffness, $S_{j,ini}$, is found not to depend on the steel grade: the joints made of S355 steel have exactly the same initial stiffness as the corresponding ones made of S700. However, the stresses in the main member lead to noticeable discrepancy in the stiffness values for different steel grades. The difference increases with the increase of n, leading to the same discrepancy in the chord stress function, $k_{sn,ip,FEM}$. As can be seen, the largest differences Δ are observed for $n = -0.99$ (16%) and $n = 0.99$ (14%).

Table 6. Validation parameters.

Main member	$100 \times 100 \times t_0$		$200 \times 200 \times t_0$	
t_0 [mm]	4	8	8	16
2γ	25	12.5	25	12.5
Connected member	$b_1 \times b_1 \times t_1$		$b_1 \times b_1 \times t_1$	
b_1 [mm]	40	90	80	180
β	0.40	0.90	0.40	0.90
Steel grade	S355, S700			
n	-0.99, -0.98, -0.95, -0.80, -0.60, -0.4, -0.2, 0, 0.2, 0.4, 0.6, 0.8, 0.95, 0.99			

At the same time, the proposed chord stress function, $k_{sn,ip}$, does not distinguish between the steel grades. Being developed for S500, it provides the results intermediate between S355 and S700, with the largest errors in the cases close to yielding (n = ±0.95…0.99). It should be noted that for the joints with other β and γ configurations, the observed errors are considerably lower, rarely exceeding 10%. Overall, the developed chord stress function provides rather accurate prediction, with the final average errors of 2.0% and 3.6% for S355 and S700 respectively.

Table 7. Validation of the chord stress function. Main member 100x100x4 (γ=25), connected member 40x40x4 (β=0.40).

n	$S_{j,ini}$ [kNm/rad]			$k_{sn,ip,FEM}$			$k_{sn,ip}$	Δ [%]	
	S355	S700	Δ [%]	S355	S700	Δ [%]		S355	S700
-0.99	21.5	18.1	16	0.71	0.59	16	0.71	0.0	19.0
-0.95	23.6	20.0	15	0.77	0.66	15	0.75	3.0	14.6
-0.80	26.6	23.0	13	0.87	0.76	13	0.84	3.5	11.3
-0.60	27.8	25.1	10	0.91	0.82	10	0.88	3.4	6.9
-0.40	28.7	27.0	6	0.94	0.89	6	0.92	2.3	4.1
-0.20	29.6	28.7	3	0.97	0.94	3	0.96	1.1	1.8
0.00	**30.4**	**30.4**	**0**	**1.00**	**1.00**	**0**	**1.00**	**0.0**	**0.0**
0.20	31.3	32.1	3	1.03	1.06	3	1.04	1.1	1.5
0.40	32.2	33.8	5	1.06	1.11	5	1.08	2.2	2.8
0.60	33.0	35.4	7	1.08	1.16	7	1.12	3.2	3.9
0.80	33.5	36.8	9	1.10	1.21	9	1.16	5.2	4.2
0.95	31.9	36.2	12	1.05	1.19	12	1.12	6.8	6.1
0.99	30.3	35.1	14	0.99	1.15	14	1.08	9.0	6.0

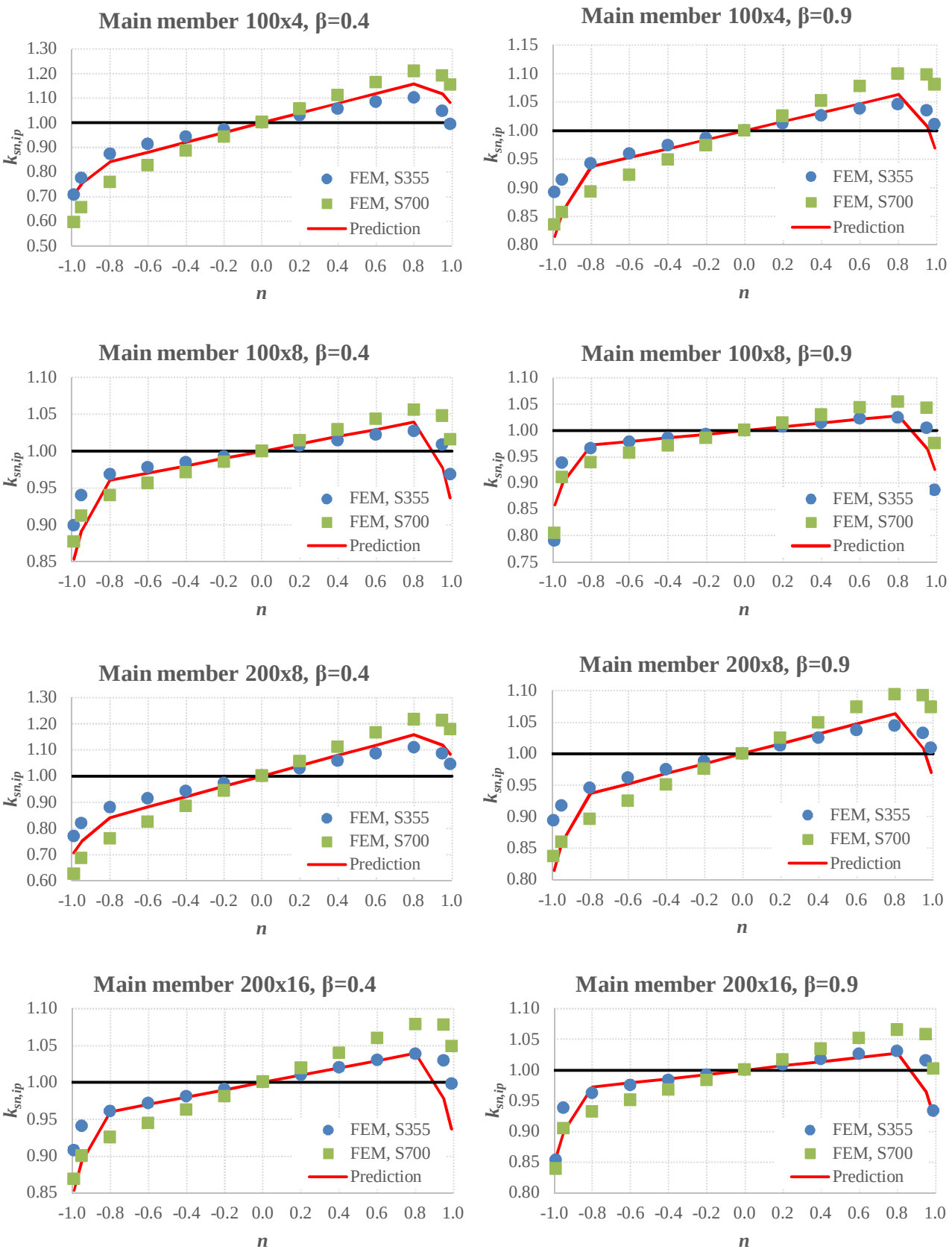

Figure 11. Validation of the proposed chord stress function.

Conclusions

This article analyzes the approach provided in [25] for analytical evaluation of the initial rotational stiffness for welded RHS T joints. By the comparison with the experimental data, it is shown that the original approach considerably underestimates the initial stiffness of the joints. To obtain more accurate results, the improved equation is proposed for the component 'main member flange in bending'. It is also found that the size of the fillet weld noticeably affects the initial rotational stiffness of the joint.

Based on the 3D FEM analysis of square hollow section joints, the axial stress in the main member is found to affect significantly their initial rotational stiffness, with the maximum decrease of stiffness by 50% for compressive loads and the maximum increase by 30% for tensile loads. The observed effect is found to depend on the brace-to-chord width ratio β and the chord width-to-thickness ratio γ.

To get reliable results in frame analyses, the chord stress function for the initial rotational stiffness of T joints is proposed, similar to that for moment resistance. The function is developed using the curve fitting technique, based on the obtained numerical results. The function is presented divided in three parts: the linear part in the range $-0.8 \leq n \leq 0.8$ and two nonlinear parts with $-0.99 \leq n < -0.8$ and $0.8 < n \leq 0.99$. The different functions are proposed for the range $0.25 \leq \beta \leq 0.85$ and $\beta = 1.0$, with the linear interpolation for $0.85 < \beta < 1.0$.

The conducted numerical validation shows that the effect of axial loads in the main member on the rotational stiffness of joints is dependent on the steel grade of the main member, which should be also included in the chord stress function as an independent variable. Generally, in the considered range, the proposed solution matches well to the numerical results and can be recommended for using in the frame design of square hollow section joints. However, more research is required to extend the function for RHS joints.

References

[1] L.M.C. Simoes, Optimization of frames with semi-rigid connections, Comput. Struct. 60(4) (1996) 531–539.

[2] D.E. Grierson, L. Xu, Design optimization of steel frameworks accounting for semi-rigid connections, , in *Optimization of Large Structural Systems, Volume II*, G. I. N. Rozvany, Ed. Dordrecht: Kluwer Academic Publisher, 1993, 873–881.

[3] K. Bzdawka, Optimization of Office Building Frame with Semi-Rigid Joints in Normal and Fire Conditions, PhD Thesis, Tampere Univ. Technol. Publ. 1038. (2012) .

[4] H. Boel, *Buckling Length Factors of Hollow Section Members in Lattice Girders. Ms Sci thesis*. Eindhoven: Eindhoven University of Technology, 2010.

[5] H.H. Snijder, H.D. Boel, J.C.D. Hoenderkamp, R.C. Spoorenberg, Buckling length factors for welded lattice girders with hollow section braces and chords, Proc. Eurosteel 2011. (2011) 1881–1886.

[6] M. Heinisuo, Ä. Haakana, Buckling of members of welded tubular truss, Nord. Steel Constr. Conf. 2015. (2015) .

[7] J. Wardenier, *Hollow Section Joints*. Delft: Delft University of Technology, 1982.

[8] (CEN) European Committee for Standardization, *Eurocode 3. Design of steel structures, Part 1–8: Design of joints (EN 1993-1-8:2005)*. Brussels, 2005.

[9] (IIW) International Institute of Welding, *ISO 14346: 2013. Static design procedure for welded*

hollow-section joints - Recommendations. 2013.

[10] M. Tabuchi, H. Kanatani, T. Kamba, The local strength of welded RHS T joints subjected to bending moment, CIDECT Rep. 5AF-84/5E. (1984) .

[11] J. Szlendak, Beam-column welded RHS connections, Thin-Walled Struct. 12(1) (1991) 63–80.

[12] J.A. Packer, Moment connections between rectangular hollow sections, J. Constr. Steel Res. 25(1–2) (1993) 63–81.

[13] Y. Yu, *The static strength of uniplanar and multiplanar connections in rectangular hollow sections*. *Doctoral Dissertation*. Delft: Delft University of Technology, 1997.

[14] L. Lu, *The static strength of I-beam to rectangular hollow section column connections*. *Doctoral Dissertation*. Delft: Delft University Press, 1997.

[15] X.L. Zhao, Deformation limit and ultimate strength of welded T-joints in cold-formed RHS sections, J. Constr. Steel Res. 53(2) (2000) 149–165.

[16] P. Ongelin, I. Valkonen, *SSAB Domex Tube. Structural hollow sections. EN 1993 - Handbook 2016*. SSAB Europe Oy, 2016.

[17] J. Wardenier, G.J. van der Vegte, D.K. Liu, Chord stress functions for K gap joints of rectangular hollow sections, Int. J. Offshore Polar Eng. 17(3) (2007) 225–232.

[18] D.K. Liu, J. Wardenier, G.J. Van Der Vegte, others, New chord stress functions for rectangular hollow section joints, Proc. Fourteenth Int. Offshore Polar Eng. Conf. (2004) 178–185.

[19] J. Wardenier, G.J. van der Vegte, D.K. Liu, Chord Stress Function for Rectangular Hollow Section X and T Joints, Proc. Seventeenth Int. Offshore Polar Eng. Conf. (2007) 3363–3370.

[20] A. Nizer, L.R.O. de Lima, P.C.G. da S. Vellasco, S.A.L. de Andrade, E. da S. Goulart, A.T. da Silva, L.F. da C. Neves, Structural behaviour of T RHS joints subjected to chord axial force, Proc. 15th Int. Symp. Tubul. Struct. Rio Janeiro, Brazil, 27-29 May 2015. (2015) 371–378.

[21] A. Lipp, T. Ummenhofer, Influence of tensile chord stresses on the strength of CHS X-joints – Experimental and numerical investigations, Proc. 15th Int. Symp. Tubul. Struct. Rio Janeiro, Brazil, 27-29 May 2015. (2015) 379–386.

[22] R.M. Korol, F.A. Mirza, Finite element analysis of RHS T-joints, J. Struct. Div. 108(9) (1982) 2081–2098.

[23] P. Mäkeläinen, R. Puthli, F. Bijlaard, Strength. stiffness and nonlinear behaviour os simple tubular joints, IABSE Congr. Rep. 13 (1988) 635–640.

[24] P. Zoetemeijer, Design Method for the Tension Side of Statically Loaded, Bolted Beam-To-Column Connections., Heron. 20(1) (1974) 1–59.

[25] D. Grotmann, G. Sedlacek, *Rotational stiffness of welded RHS beam-to-column joints. Cidect 5BB-8/98*. Aachen: RWTH-Aachen, 1998.

[26] K. Weynand, J.P. Jaspart, .J-F. Demonceau, L. Zhang, *Component method for tubular joints. CIDECT Report 16F – 3/15*. 2015.

[27] J. Packer, R. Puthli, G.J. van der Vegte, J. Wardenier, Discussion on the paper “Experimental and numerical assessment of RHS T-joints subjected to brace and chord axial forces”, by Nizer et al., Steel Construction 9 (2016), No. 4, pages 315–322., Steel Constr. 10(1) (2017) 89–90.

[28] M. Heinisuo, H. Perttola, H. Ronni, A step towards the 3D component method for modelling

beam-to-column joints, Steel Constr. 7(1) (2014) 8–13.

[29] A.A. Del Savio, D.A. Nethercot, P.C.G.S. Vellasco, S.A.L. Andrade, L.F. Martha, Generalised component-based model for beam-to-column connections including axial versus moment interaction, J. Constr. Steel Res. 65(8–9) (2009) 1876–1895.

[30] K.W. Johansen, *Brudlinieteorier*. Copenhagen: Forlag, 191 pp. (Yield Line theory, Translated by Cement and Concrete Association, London, 1962. 181 pp.), 1943.

[31] A.D. Christitsas, D.T. Pachoumis, C.N. Kalfas, E.G. Galoussis, FEM analysis of conventional and square bird-beak SHS joint subject to in-plane bending moment — experimental study, J. Constr. Steel Res. 63(10) (2007) 1361–1372.

[32] J. Havula, H. Myllymäki, I. Sorsa, J. Haapio, M. Heinisuo, Experimental research of welded tubular HSS T-joints, welding times and moment resistances, IIW International Conference High Strength Materials - Challenges and Applications, 2015, .

[33] F. Mang, Ö. Bucak, Hohlprofilkonstruktionen, Stahlbauhandbuch, Stahlbau-Verlag-GmbH Köln. (1982) .

[34] H. Kanatani, K. Fujiwara, M. Tabuchi, T. Kamba, *Bending tests on T-joints of RHS chord and RHS or H-shape branch. CIDECT Programme 5AF*. 1981.

[35] M. Heinisuo, M. Garifullin, T. Jokinen, T. Tiainen, K. Mela, Surrogate modeling for rotational stiffness of welded tubular Y-joints, Proc. Eighth Int. Work. Connect. Steel Struct. (Connections VIII). (2016) .

[36] M. Garifullin, S. Pajunen, K. Mela, M. Heinisuo, 3D component method for welded tubular T joints, Int. Symp. Tubul. Struct. Melbourne, Aust. 4-6 December 2017. Submitt. (2017) .

[37] *Abaqus 6.12*. *Getting Started with Abaqus: Interactive Edition*. Dassault Systèmes, 695 p., 2012.

[38] (CEN) European Committee for Standardization, *Cold formed welded structural hollow sections of non-alloy and fine grain steels. Part 2: Tolerances, dimensions and sectional properties (EN 10219-2:2006)*. Brussels, 2006.

[39] G.J. van der Vegte, Y. Makino, Further research on chord length and boundary conditions of CHS T- and X-joints, Adv. Steel Constr. 6(3) (2010) 879–890.

[40] Ä. Haakana, *In-Plane Buckling and Semi-Rigid Joints of Tubular High Strength Steel Trusses. Ms Sci thesis*. Tampere: Tampere University of Technology, 2014.

[41] H. AlHendi, M. Celikag, Behavior of reverse-channel and double-reverse-channel connections to tubular columns with HSS, J. Constr. Steel Res. 112 (2015) 271–281.